 https://doi.org/10.3311/PPee.22464

Periodica Polytechnica Electrical Engineering and Computer Science, 68(1), pp. 12–20, 2024

Active Fault-tolerant Control for Surface Permanent Magnet Synchronous Motor Under Demagnetization Fault

Ayyoub Zeghlache[1*], Hemza Mekki[1], Ali Djerioui[1], Mohamed Fouad Benkhoris[2]

[1] Electrical Engineering Laboratory (LGE), Department of Electrical Engineering, Faculty of Technology, University of M'Sila, 28000 M'Sila, El Hodna, P.O.B. 18, Algeria
[2] IREENA Laboratory, Department of Electrical Engineering, University of Nantes, 44602 St-Nazaire, P.O.B. 406, France
[*] Corresponding author, e-mail: ayyoub.zeghlache@univ-msila.dz

Received: 24 April 2023, Accepted: 06 September 2023, Published online: 03 November 2023

Abstract

This paper introduces a novel method for controlling a surface permanent magnet synchronous motor (SPMSM) during demagnetization fault conditions. The proposed fault-tolerant control (FTC) system incorporates a combination of a fuzzy extended state observer (FESO) based on an interval type 2 fuzzy logic controller (IT2FLC) and second-order sliding mode control (SOSMC) utilizing the super-twisting algorithm. The FESO aims to identify and eliminate demagnetization faults through reconstruction control. The FTC system enhances the dynamic performance and disturbance rejection of the SPMSM, providing a robust solution in the event of a demagnetization fault.

Keywords

fault-tolerant control, surface permanent magnet synchronous motor, second-order sliding mode control, extended state observer, interval type 2 fuzzy logic controller

1 Introduction

The use of field-oriented control is on the rise to enhance the dynamic performance of permanent magnet synchronous motors (PMSMs), especially those with simple construction, such as surface permanent magnet synchronous motors (SPMSMs). Various applications commonly use SPMSMs, including electric vehicles, aircraft, and trucks [1]. It is essential to provide adequate support for these systems and ensure they can still function even in the event of faults.

SPMSMs are susceptible to demagnetization faults, which can significantly reduce their efficiency as they are composed of permanent magnets. Demagnetization faults can arise due to environmental factors and electromagnetic fields. According to [2], an operational environment with a high temperature of 100 °C can result in a 20% reduction in permanent magnet flux.

A design technique named fault-tolerant control (FTC) has recently been widely used for allowing systems like motors to continue operating in the event of a fault. Numerous effective FTC algorithms have recently emerged in the literature to improve the performance of motor systems under fault conditions. In [3], researchers developed a fault-tolerant control for motor systems using a first-order sliding mode observer (SMO) that detects and eliminates faults in real time. Another design in [4] incorporates the estimation of the effect of demagnetization faults in a permanent magnet synchronous motor (PMSM) by using an improved SMO algorithm based on equivalent input disturbance (EID). However, the main challenge with SMO algorithms is the requirement of bounded and differentiable uncertainties.

Han [5] proposed the extended state observer (ESO) approach to address disturbances and unknown terms as extra states in the system to be estimated. This method has proven effective in various fields, including load torque identification and fault-tolerant controls. In [6], authors proposed a fault-tolerant control based on extended state observers to handle open circuit faults in the switch of the five-leg converter and the phase of 5-phase permanent magnet synchronous generators, aiming to maintain system stability and robustness despite faults. In [7], a control technique combines sliding-mode control (SMC) and an extended state observer (ESO) to achieve fast speed-tracking performance while considering all disturbances, including load torque.

This paper presents a proposed strategy for the FTC that combines the second-order sliding mode control (SOSMC) discussed in [8–10] with a fuzzy extended state

Cite this article as: Zeghlache, A., Mekki, H., Djerioui, A., Benkhoris, M. F. "Active Fault-tolerant Control for Surface Permanent Magnet Synchronous Motor Under Demagnetization Fault", Periodica Polytechnica Electrical Engineering and Computer Science, 68(1), pp. 12–20, 2024.
https://doi.org/10.3311/PPee.22464

observer (FESO) incorporating an interval type 2 fuzzy logic controller (IT2FLC) [11]. This FTC method aims to ensure the robust operation of a surface permanent magnet synchronous motor (SPMSM) despite a permanent magnet demagnetization fault. The paper highlights the following key contributions:

- A speed and *dq*-frame current controller for PMSMs based on a SOSMC, aiming to improve the control performance and stability of the PMSM system.
- The combination of speed and current controllers with an observer based on the IT2FLC provides a robust system for addressing comprehensive disturbances that affect the performance of the SPMSM, such as parameter variations and load torque. This approach offers enhanced control and stability, ensuring the effectiveness of the system.
- Demonstrating the efficiency and robust dynamic performance of the speed and current controllers through a FTC approach based on the FESO, specifically in handling demagnetization fault.

The organization of the remaining five sections is as follows. Section 2 concisely gives the SPMSM model and illustrates how it adapts when disturbances occur. Section 3 introduces the SOSMC and the stability proof. Section 4 describes the SPMSM model with demagnetization fault and presents the proposed FTC, designed based on a FESO. Finally, Sections 5 and 6 present the simulation results and the conclusion of the paper, respectively.

2 SPMSM modeling

The PMSM stator voltage equations are as follows (Eq. (1)):

$$\begin{cases} V_d = R_s i_d + \dfrac{d\Phi_d}{dt} - n_p \Omega \Phi_q \\ V_q = R_s i_q + \dfrac{d\Phi_q}{dt} + n_p \Omega \Phi_d \end{cases}. \tag{1}$$

The stator flux equations are as follows (Eq. (2)):

$$\begin{cases} \Phi_d = L_d i_d + \Phi_f \\ \Phi_q = L_q i_q \end{cases}. \tag{2}$$

The PMSM produces torque according to Eq. (3):

$$\begin{aligned} T_{em} &= \frac{3}{2} n_p \left(\Phi_d i_q - \Phi_q i_d \right) \\ &= \frac{3}{2} n_p \left[\left(L_d - L_q \right) i_d i_q + \Phi_f i_q \right]. \end{aligned} \tag{3}$$

With SPMSM machine attributes ($L_d = L_q = L_s$), the simplified expression is as follows (Eq. (4)):

$$T_{em} = \frac{3}{2} n_p \Phi_f i_q. \tag{4}$$

To facilitate the development of control laws for the SPMSM and enhance understanding of its *dq*-frame dynamic model, the expressions of the substitution of the stator flux equations (Eq. (2)) into the voltage equations (Eq. (1)) are as follows (Eq. (5)):

$$\begin{cases} \dfrac{d_{id}}{dt} = c_1 i_d + n_p \Omega i_q + \beta V_d \\ \dfrac{d_{iq}}{dt} = c_1 i_q - n_p \Omega i_d + c_2 \Omega + \beta V_q \\ \dfrac{d\Omega}{dt} = c_3 i_q - \alpha_1 \Omega - \alpha_2 T_r \end{cases}. \tag{5}$$

The components of the SPMSM model (Eq. (5)) express consistently with the machine parameters as follows:

$$c_1 = -\frac{R_s}{L_s},\ c_2 = -\frac{n_p \Phi_f}{L_s},\ c_3 = \frac{3 n_p \Phi_f}{2J},$$
$$\alpha_1 = \frac{f}{J},\ \alpha_2 = \frac{1}{J},\ \beta = \frac{1}{L_s},$$

where V_d, V_q, i_d and i_q represent the stator voltages and currents of *dq*-frame, respectively; L_s is the inductance of *dq*-frame, respectively; R_s is the stator resistance; Φ_f is the rotor flux; Ω is the rotor speed; J is the moment of inertia; f denote friction coefficient and T_r represents the load torque; n_p is the pole pairs number of the motor.

Considering the load disturbances and perturbation parameters, the SPMSM model (Eq. (5)) can be expressed as follows (Eq. (6)):

$$\begin{cases} \dfrac{d_{id}}{dt} = c_1 i_d + n_p \Omega i_q + \beta V_d + d_{id} \\ \dfrac{d_{iq}}{dt} = c_1 i_q - n_p \Omega i_d + c_2 \Omega + \beta V_q + d_{iq} \\ \dfrac{d\Omega}{dt} = c_3 i_q - \alpha_1 \Omega + d_\Omega \end{cases}, \tag{6}$$

where d_{id}, d_{iq} and d_Ω are the lumped disturbances given as follows (Eq. (7)):

$$\begin{pmatrix} d_{id} \\ d_{iq} \\ d_\Omega \end{pmatrix} = \begin{pmatrix} \Delta c_1 i_d + \Delta \beta V_d \\ \Delta c_1 i_q + \Delta c_2 \Omega + \Delta \beta V_q \\ \Delta c_3 \Omega - \Delta \alpha_1 \Omega - \alpha_2 T_r - \Delta \alpha_2 \Delta T_r \end{pmatrix}. \tag{7}$$

The components of the lumped disturbances (d_{id}, d_{iq}, d_{Ω}) represent as follows:

$$\Delta c_1 = -\frac{\Delta R_s}{\Delta L_s},\ \Delta c_2 = -\frac{n_p \phi_f}{\Delta L_s},\ \Delta c_3 = \frac{3 n_p \phi_f}{2 \Delta J},$$
$$\Delta \alpha_1 = \frac{\Delta f}{\Delta J},\ \Delta \alpha_2 = \frac{1}{\Delta J},\ \Delta \beta = \frac{1}{\Delta L_s},$$

where ΔR_s, ΔL_s, ΔJ and Δf represents the variations in motor parameter values.

3 Second-order sliding mode control

The definition of the SOSMC law, based on a super-twisting algorithm, is as follows [12] (Eq. (8)):

$$\begin{cases} \dot{s} = -k_1 \sqrt{|s|} \operatorname{sign}(s) + U + \rho_1 \\ \dot{U} = -k_2 \operatorname{sign}(s) + \rho_2 \end{cases}, \tag{8}$$

where s is the sliding surface; k_1 and k_2 are positive constants; ρ_1 and ρ_2 are perturbation terms.

We define the following sliding surfaces (Eq. (9)):

$$\begin{aligned} S_1 &= \Omega - \Omega_{ref} \\ S_2 &= i_q - i_{q_{ref}} \\ S_3 &= i_d - i_{d_{ref}} \end{aligned}. \tag{9}$$

The SOSMC laws for the speed and currents in the dq-frame controllers are given below (Eqs. (10) to (12)):

$$\begin{cases} i_{q_{ref}} = \dfrac{1}{c_3}\left(\alpha_1 \Omega + \dot{\Omega}_{ref}\right) - k_{1\Omega} \sqrt{|s_1|} \operatorname{sign}(s_1) + U_{\Omega} \\ \dot{U}_{\Omega} = -k_{2\Omega} \operatorname{sign}(s_1) \end{cases}, \tag{10}$$

$$\begin{cases} V_{q_{ref}} = \dfrac{1}{\beta}\left(-c_1 i_q + n_p \Omega i_d - c_2 \Omega + \dot{i}_{q_{ref}}\right) \\ \qquad -k_{1q} \sqrt{|s_2|} \operatorname{sign}(s_2) + U_q \\ \dot{U}_q = -k_{2q} \operatorname{sign}(s_2) \end{cases}, \tag{11}$$

$$\begin{cases} V_{d_{ref}} = \dfrac{1}{\beta}\left(-c_1 i_d - n_p \Omega i_q + \dot{i}_{d_{ref}}\right) \\ \qquad -k_{1d} \sqrt{|s_3|} \operatorname{sign}(s_3) + U_d \\ \dot{U}_d = -k_{2d} \operatorname{sign}(s_3) \end{cases}, \tag{12}$$

3.1 Stability analysis

The Lyapunov function is defined as follows [12] (Eq. (13)):

$$V = 2k_2 |s| + \frac{1}{2} U^2 + \frac{1}{2}\left(k_1 |s|^{1/2} \operatorname{sign}(s) - U\right)^2. \tag{13}$$

The proposed Lyapunov function can also be expressed in quadratic form as follows (Eq. (14)):

$$V = \zeta^T P \zeta, \tag{14}$$

where:

$$\zeta^T = \begin{bmatrix} |s|^{1/2} \operatorname{sign}(s) & U \end{bmatrix}$$
$$P = \frac{1}{2}\begin{bmatrix} 4k_2 + k_1^2 & -k_1 \\ -k_1 & 2 \end{bmatrix}.$$

Taking the time derivative of Eq. (14) yields:

$$\dot{V} = -\frac{1}{2} k_1 |s|^{-1/2} \zeta^T q \zeta, \tag{15}$$

where:

$$q = \frac{k_1}{2}\begin{bmatrix} 2k_2 + k_1^2 & -k_1 \\ -k_1 & 1 \end{bmatrix}.$$

The perturbation terms are as follows: $\rho_{1\Omega} = d_{\Omega}$, $\rho_{1q} = d_{iq}$, $\rho_{1d} = d_{id}$. It should be noted that the second terms, $\rho_{2\Omega}$, ρ_{2q} and ρ_{2d}, do not exist and are equal to zero. The perturbation terms are globally bounded, as follows (Eq. (16)):

$$\begin{aligned} |\rho_{1\Omega}| &\le \delta_{\Omega} \sqrt{|s_1|} \\ |\rho_{1q}| &\le \delta_q \sqrt{|s_2|} \\ |\rho_{1d}| &\le \delta_d \sqrt{|s_3|} \end{aligned}, \tag{16}$$

where δ_{Ω}, δ_q and δ_d are bounding known positive constants. To ensure the stability of the system ($\dot{V} < 0$), we must select control gains that satisfy the following conditions:

$$\begin{cases} k_{1\Omega} > 2\delta_{\Omega} \\ k_{2\Omega} > k_{1\Omega} \dfrac{5\delta_{\Omega} k_{1\Omega} + 4\delta_{\Omega}^2}{2\left(k_{1\Omega} - 2\delta_{\Omega}\right)} \end{cases}$$
$$\begin{cases} k_{1q} > 2\delta_q \\ k_{2q} > k_{1q} \dfrac{5\delta_q k_{1q} + 4\delta_q^2}{2\left(k_{1q} - 2\delta_q\right)} \end{cases}. \tag{17}$$
$$\begin{cases} k_{1d} > 2\delta_d \\ k_{2d} > k_{1d} \dfrac{5\delta_d k_{1d} + 4\delta_d^2}{2\left(k_{1d} - 2\delta_d\right)} \end{cases}$$

3.2 Chattering attenuation

A significant limitation of the sliding mode technique is the occurrence of chattering, which can be attributed to using the sign function. Experts suggest substituting the sign function with the sigmoid function to reduce chattering. The sigmoid function is given by [13]:

$$F = \frac{s}{|s| + m}, \tag{18}$$

where m is a small positive value, such as: $|s| >> m$.

4 FTC based on FESO

The proposed FTC of the SPMSM utilizes fuzzy extended state observers for fault detection and reconstruction, as illustrated in Fig. 1.

4.1 SPMSM model in demagnetization faulty condition

External factors, such as elevated temperatures, can induce the permanent loss of magnetic properties in magnets. In the event of a demagnetization fault, the amplitude and direction of the flux linkage in permanent magnets will vary. These variations are illustrated in Fig. 2, where the flux linkage amplitude transitions from Φ_f to Φ_r, accompanied by a deviation angle represented as γ.

In the case that the permanent magnets demagnetization fault occurs, the rotor flux linkage will become:

$$\begin{cases} \Phi_d = L_d i_d + \Phi_f + \Delta\Phi_{rd} \\ \Phi_q = L_q i_q + \Delta\Phi_{rq} \end{cases}, \tag{19}$$

where $\Delta\Phi_{rd} = \Phi_r \cos\gamma - \Phi_f$ and $\Delta\Phi_{rd} = \Phi_r \sin\gamma$ represent perturbation values for flux linkage components along the dq-frame.

The electromagnetic torque Eq. (4) will become as follows in Eq. (20):

$$T_{em} = \frac{3}{2} n_p \Phi_f i_q + \frac{3}{2} n_p \left(\Delta\Phi_{rd} i_q - \Delta\Phi_{rq} i_d\right). \tag{20}$$

Substituting Eq. (19) into Eq. (1) gives the state equation for a demagnetized SPMSM:

$$\begin{cases} \dfrac{d_{id}}{dt} = c_1 i_d + n_p \Omega i_q + \beta V_d + f_d \\ \dfrac{d_{iq}}{dt} = c_1 i_q - n_p \Omega i_d + c_2 \Omega + \beta V_q + f_q \\ \dfrac{d\Omega}{dt} = c_3 i_q - \alpha_1 \Omega + f_\Omega \end{cases}, \tag{21}$$

with:

$$\begin{pmatrix} f_d \\ f_q \\ f_\Omega \end{pmatrix} = \begin{pmatrix} \dfrac{n_p}{L_s} \Delta\Phi_{rq} \Omega \\ -\dfrac{n_p}{L_s} \Delta\Phi_{rd} \Omega \\ \dfrac{3n_p}{2J}\left(\Delta\Phi_{rd} i_q - \Delta\Phi_{rq} i_d\right) - \alpha_2 T_r \end{pmatrix}.$$

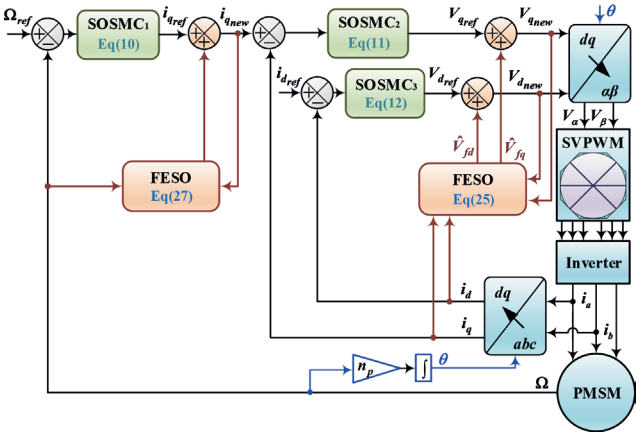

Fig. 1 Structural diagram of the proposed FTC

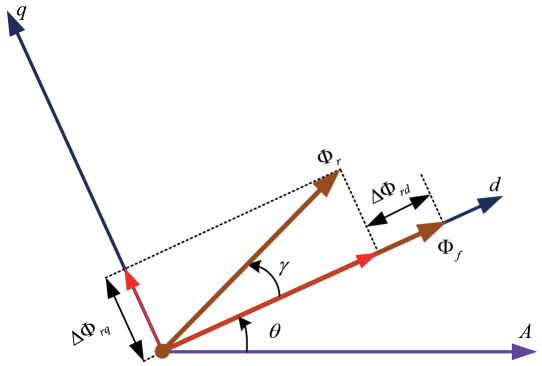

Fig. 2 Variation of PMSM flux-linkage

4.2 Fuzzy ESO

To design an ESO observer for the SPMSM, it is necessary to establish a model of the motor. It can be defined using the state equations shown below:

$$\begin{cases} \dot{x} = A\boldsymbol{x}(t) + Bu(t) + D\dot{\boldsymbol{f}}(t) \\ y = C\boldsymbol{x}(t) \end{cases}. \tag{22}$$

According to the state Eq. (22), the traditional ESO of the SPMSM is designed as follows:

$$\dot{\hat{\boldsymbol{x}}}(t) = A\hat{\boldsymbol{x}}(t) + B\boldsymbol{u}(t) + D\dot{\hat{\boldsymbol{f}}}(t) + \boldsymbol{h}\left(\boldsymbol{y}(t) - \hat{\boldsymbol{y}}(t)\right), \tag{23}$$

where $\hat{\boldsymbol{x}}(t)$, $\hat{\boldsymbol{y}}(t)$ and $\hat{\boldsymbol{f}}(t)$ are the estimates of $\boldsymbol{x}(t)$, $\boldsymbol{y}(t)$ and $\boldsymbol{f}(t)$, respectively; $\boldsymbol{h}$ is the observer gain matrix.

The following extended state-space model can describe the stator current of SPMSM:

$$\begin{aligned} \frac{d}{dt}\begin{bmatrix} i_d \\ i_q \\ f_d \\ f_q \end{bmatrix} &= \begin{bmatrix} c_1 & n_p\Omega & 1 & 0 \\ -n_p\Omega & c_1 & 0 & 1 \\ 0 & 0 & 0 & 0 \\ 0 & 0 & 0 & 0 \end{bmatrix}\begin{bmatrix} i_d \\ i_q \\ f_d \\ f_q \end{bmatrix} + \begin{bmatrix} 0 \\ c_2\Omega \\ 0 \\ 0 \end{bmatrix} \\ &+ \begin{bmatrix} \beta & 0 \\ 0 & \beta \\ 0 & 0 \\ 0 & 0 \end{bmatrix}\begin{bmatrix} V_d \\ V_q \end{bmatrix} + \begin{bmatrix} 0 & 0 \\ 0 & 0 \\ 1 & 0 \\ 0 & 1 \end{bmatrix}\begin{bmatrix} \dot{f}_d \\ \dot{f}_q \end{bmatrix}, \end{aligned} \tag{24}$$

where $\boldsymbol{x}(t) = [i_d\ i_q\ f_d\ f_q]^T$ is the state vector; $\boldsymbol{u}(t) = [V_d\ V_q]^T$ is the control vector; $\boldsymbol{y} = [i_d\ i_q]^T$ is the output vector; $\boldsymbol{f}(t) = [f_d\ f_q]^T$ represents the demagnetization fault affecting the SPMSM.

It is clear that system Eq. (24) has full rank and is observable. It is possible to get the equations of the fuzzy ESO for the currents as follows:

$$\begin{cases} \dot{\hat{i}}_d = c_1\hat{i}_d + n_p\Omega\hat{i}_q + \hat{f}_d + \beta V_d + h_{d1}\mathrm{FLC}_d \\ \dot{\hat{f}}_d = h_{d2}\mathrm{FLC}_d \\ \dot{\hat{i}}_q = -n_p\Omega\hat{i}_d + c_1\hat{i}_q + \hat{f}_q + \beta V_q + h_{q1}\mathrm{FLC}_q \\ \dot{\hat{f}}_q = h_{q2}\mathrm{FLC}_q \end{cases}, \tag{25}$$

where h_{d1}, h_{d2}, h_{q1} and h_{q2} are constants that are all positive; $\hat{f}_d$ and $\hat{f}_q$ are the estimates of f_d and f_q, respectively.

The extended state-space model for the speed of SPMSM can be expressed as:

$$\frac{d}{dt}\begin{bmatrix}\Omega \\ f_\Omega\end{bmatrix} = \begin{bmatrix}-\alpha_1 & 1 \\ 0 & 0\end{bmatrix}\begin{bmatrix}\Omega \\ f_\Omega\end{bmatrix} + \begin{bmatrix}c_3 \\ 0\end{bmatrix} i_q + \begin{bmatrix}0 \\ 1\end{bmatrix}\dot{f}_\Omega, \tag{26}$$

where $\boldsymbol{x}(t) = [\Omega\ \ f_\Omega]^T$ is the state vector; $\boldsymbol{u}(t) = i_q$ is the input; $\boldsymbol{y} = \Omega$ is the output; $\boldsymbol{f}(t) = f_\Omega$ denotes the total perturbation amount resulting from the load and demagnetization fault.

The equation of the fuzzy ESO for the speed can be obtained by:

$$\begin{cases} \dot{\hat{\Omega}} = -\alpha_1\hat{\Omega} + \hat{f}_\Omega + c_3 i_q + h_{\Omega 1}\mathrm{FLC}_\Omega \\ \dot{\hat{f}}_\Omega = h_{\Omega 2}\mathrm{FLC}_\Omega \end{cases}, \tag{27}$$

where $h_{\Omega 1}$ and $h_{\Omega 2}$ are both positive constants.

The IT2FLC operates by using the error signal ($i_d - \hat{i}_d$, $i_q - \hat{i}_q$, $\Omega - \hat{\Omega}$) as its input and applying proportional, integral, and derivative control actions to produce the output as follows:

$$\begin{cases} \mathrm{FLC}_d = K_{pd}\varphi_{pd} + K_{id}\varphi_{id} + K_{dd}\varphi_{dd} \\ \mathrm{FLC}_q = K_{pq}\varphi_{pq} + K_{iq}\varphi_{iq} + K_{dq}\varphi_{dq} \\ \mathrm{FLC}_\Omega = K_{p\Omega}\varphi_{p\Omega} + K_{i\Omega}\varphi_{i\Omega} + K_{d\Omega}\varphi_{d\Omega} \end{cases}, \tag{28}$$

where K_{pd}, K_{pq} and $K_{p\Omega}$ are the gains of the proportional controller. K_{id}, K_{iq} and $K_{i\Omega}$ are the gains of the integral controller. K_{dd}, K_{dq} and $K_{d\Omega}$ are the gains of the derivative controller. φ_d, φ_q and φ_Ω are the outputs of the interval type 2 fuzzy logic control given by Eq. (31).

As shown in Fig. 3, the input scaling factor (K_e) is chosen to normalize the input to the range of [−1, 1], which is the same range as the membership functions of the IT2FLC depicted in Fig. 4 [14].

The IT2FLC has the following rule structure [11]:

$$R_i:\ \text{if } \sigma \text{ is } \tilde{A}_i,\ \text{then } \varphi \text{ is } B_i,\ i = 1,2,3, \tag{29}$$

where B_i are crisp outcomes, with the specific values of $B_1 = -1$, $B_2 = 0$ and $B_3 = 1$. m_1, m_2 and m_3 represent the height of the lower membership functions and are defined as follows:

$$\begin{cases} m_1 = m_3 = 1 - \alpha \\ m_2 = \alpha \end{cases}. \tag{30}$$

Therefore, the only parameter that needs to be adjusted in IT2FLC is α [11].

The formula for the fuzzy mapping of the single input IT2FLC, denoted as $\varphi(\sigma)$, was presented in [11] and can be expressed as follows:

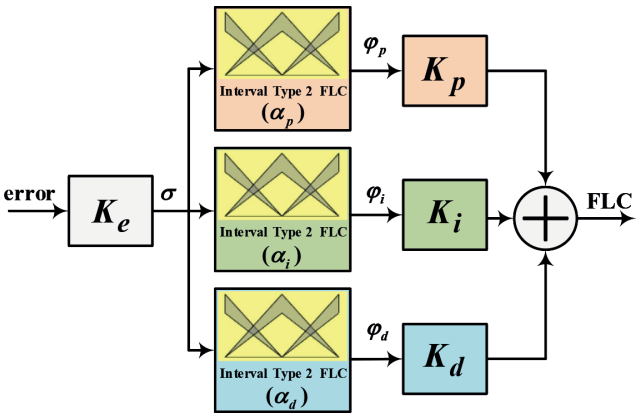

Fig. 3 Structure of the IT2FLC

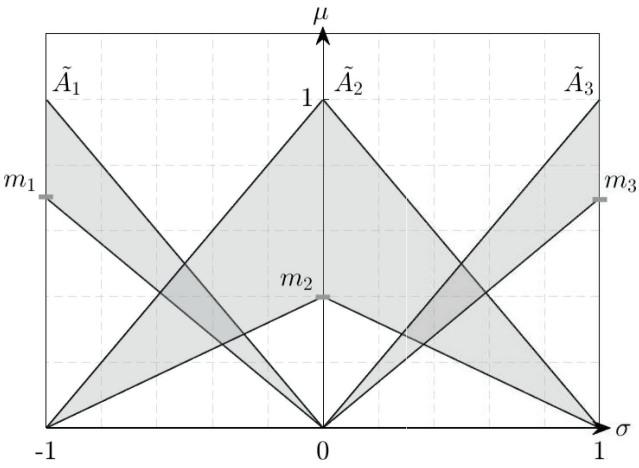

Fig. 4 Membership functions

$$\varphi(\sigma)=\sigma k(|\sigma|), \tag{31}$$

where $k(\sigma)$ is the nonlinear gain, which is defined as follows:

$$k(\sigma)=\frac{1}{2}\left(\frac{1}{\alpha+\sigma-\alpha\sigma}+\frac{\alpha-1}{\alpha\sigma-1}\right). \tag{32}$$

4.3 Reconstruction control

The proposed fault-tolerant control uses new control laws shown as follows:

$$\begin{cases} i_{q_{new}}=i_{qref}+\hat{i}_{fq} \\ V_{d_{new}}=V_{dref}+\hat{V}_{fd} \\ V_{q_{new}}=V_{qref}+\hat{V}_{fq} \end{cases}, \tag{33}$$

where i_{qref}, V_{qref} and V_{dref} are the SOSMC control laws given by Eq. (10), Eq. (11), and Eq. (12); respectively, the additional control laws $\hat{i}_{fq}$, $\hat{V}_{fd}$ and $\hat{V}_{fq}$ are determined by a fuzzy ESO that estimates the impact of the demagnetization fault and are defined as:

$$\begin{cases} \hat{i}_{fq}=-\frac{1}{c_3}\hat{f}_{\Omega} \\ \hat{V}_{fd}=-\frac{1}{\beta}\hat{f}_{d} \\ \hat{V}_{fq}=-\frac{1}{\beta}\hat{f}_{q} \end{cases}, \tag{34}$$

where $\hat{f}_{\Omega}$, $\hat{f}_{d}$ and $\hat{f}_{q}$ are the fault estimates computed through Eq. (27) and Eq. (25).

5 Simulation results

A simulation model for a SPMSM was implemented and tested using MATLAB/Simulink [15]. The model utilizes the structural diagram of the proposed FTC (Fig. 1) with $i_{dref}=0$. The parameters for the SPMSM drive are outlined in Table 1.

Processor-in-the-loop (PIL) experimentation is a useful way to evaluate the control system on hardware, as it allows the control algorithm to be considered in real-time. The controller validated through PIL testing was equally efficient when tested on actual hardware [16]. To verify the proposed control, a PIL experiment was conducted, and its setup is shown in Fig. 5. The Simulink model had a fixed step size of 1×10^{-6} s and was run using Simulink rapid prototyping on a dual-core DSP board (TMS320F28069M). The SPMSM and inverter systems were not physically present but simulated in Simulink, with the controller operating in real-time.

Table 1 Parameters of the SPMSM drive

Parameter	Value
Rated output power (P_{rated})	4.4 kW
Rated speed (n_{rated})	1500 rpm
Rated torque (T_{rated})	28.4 Nm
Rated current (I_{rated})	16.5 A
Rated voltage (V_{rated})	400 V
Pole pairs (n_p)	4
Stator resistance (R_s)	0.25 Ohm
Stator inductance (L_s)	4.8 mH
PM flux-linkage (ϕ_f)	0.32 Wb
Inertia constant (J)	0.00774 Kg × m^2
Viscous friction (f)	0.0089 Kg × m^2/s

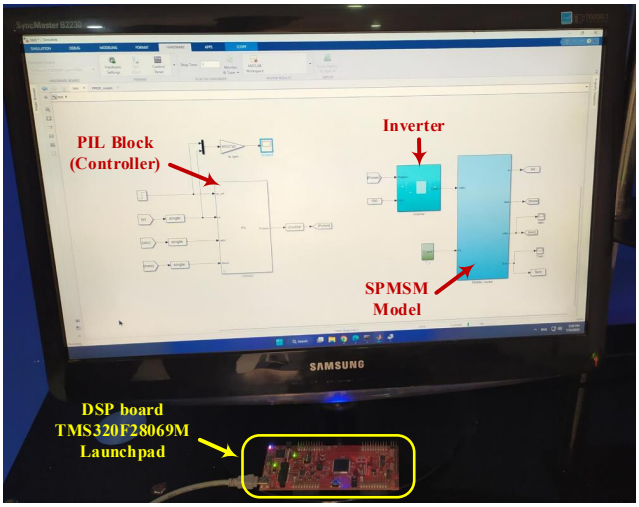

Fig. 5 Experimental DSP board

A simulation test was conducted to assess the performance of the proposed control strategy for SPMSM, and the results were compared with PI control and conventional SMC. The conventional SMC employed the same sliding surfaces as the SOSMC design, but it also needed to estimate the load torque by using Eq. (35):

$$\dot{\hat{T}}_r=-\eta S_1 \quad \eta>0. \tag{35}$$

Table 2 summarizes the parameters of the controllers and observers.

5.1 SPMSM under healthy conditions

The efficacy of the SOSMC was tested through an experiment conducted on a SPMSM under normal operating conditions, with variations in speed and torque. Fig. 6(a) presents the variation in load torque, which began with a speed reference of 1500 rpm and a rated load torque of 28.4 Nm. At 0.4 s, the motor experienced a sudden increase in torque to 38.4 Nm before returning to its initial value of 28.4 Nm at 0.8 s. Fig. 6(b) presents the variation in speed

Table 2 Parameters of the controllers and observers

Speed	q-axis current	d-axis current
$k_{1\Omega} = 80$	$k_{1q} = 100$	100
$k_{2\Omega} = 600$	$k_{2q} = 600$	600
$h_{\Omega 1} = 500$	$h_{q1} = 800$	$h_{d1} = 1000$
$h_{\Omega 2} = 90000$	$h_{q2} = 640000$	$h_{d2} = 500000$
$K_e = 1/11$	$K_e = 1/95$	$K_e = 1/13$
$K_{p\Omega} = 11$	$K_{pq} = 95$	$K_{pd} = 13$
$K_{i\Omega} = 9$	$K_{iq} = 85$	$K_{id} = 8$
$K_{d\Omega} = 6$	$K_{dq} = 70$	$K_{dd} = 9$
$\alpha_p = 0.62$	$\alpha_p = 0.5$	$\alpha_p = 0.25$
$\alpha_i = 0.075$	$\alpha_i = 0.9$	$\alpha_i = 0.5$
$\alpha_d = 0.62$	$\alpha_d = 0.5$	$\alpha_d = 0.5$

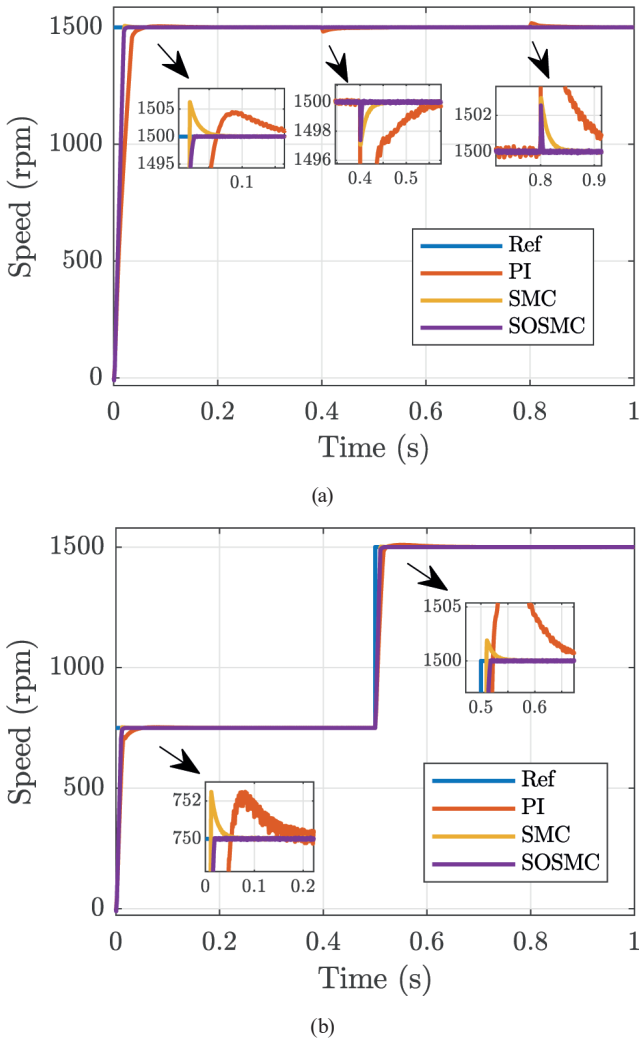

Fig. 6 Speed performance under healthy conditions; (a) Variation in load torque; (b) Variation in speed reference

reference, which started at 750 rpm at time 0 s and reached its nominal value of 1500 rpm at 0.5 s.

Fig. 6 compares the speed responses to sudden changes in load torque and speed reference among three control techniques: PI control, traditional SMC, and SOSMC. The comparison highlights that the speed response of SOSMC demonstrated the lowest amount of oscillation and fluctuation in the speed response compared to the other two methods. Furthermore, the response of PI control was slower in tracking the reference speed compared to SMC and SOSMC. Conversely, SOSMC achieved a quicker settling time to attain a steady state, less overshooting, and without requiring load torque estimation.

5.2 SPMSM under demagnetization fault

The simulation of permanent-magnet demagnetization was carried out by altering the permanent-magnet amplitude (Φ_r) and the deviation angle (γ). As illustrated in Fig. 7, the reference speed was 1500 rpm, while the load torque was 20 Nm. The amplitude of the permanent-magnet flux was 0.32 Wb at 0 s and 0.25 Wb at 0.5 s, while the deviation angle was 0 degrees at 0 s and 60 degrees at

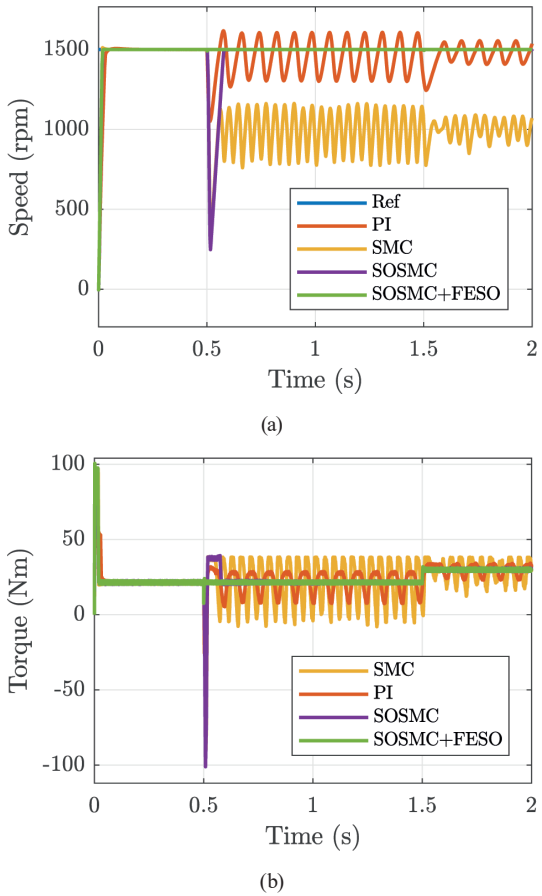

Fig. 7 Speed and torque performance under demagnetization fault; (a) Speed response; (b) Torque response

0.3 s. The load torque changed from 20 Nm to 28.4 Nm at $t = 1.5$ s to evaluate the fault-tolerant control under demagnetization fault.

Fig. 7 demonstrates that SOSMC remains powerful in both healthy and faulty conditions compared to PI control and traditional SMC. However, it still experiences fluctuations during transitions when a fault occurs. By boosting SOSMC with FESO, the performance of SOSMC in handling permanent magnet demagnetization faults is improved. This enhancement provides strong robustness and compensates for uncertainties and faults.

Figs. 8 and 9 compare the simulation results of the traditional ESO and the FESO regarding their ability to estimate f_Ω, f_d and f_q values. The traditional ESO exhibits oscillatory behavior in its estimate, while the FESO produces a smoother estimate. This indicates that the FESO can generate more stable and reliable estimates than its conventional counterpart when a demagnetization fault occurs. This finding highlights the robustness and effectiveness of the interval type 2 fuzzy logic-based approach in addressing the uncertainties and nonlinearities inherent in the system. Mean square error values for the estimation data in Figs. 8 and 9 are presented in Table 3.

6 Conclusion

This paper presented a FTC based on SOSMC with FESO for electric motor systems. The proposed control addressed the challenges of disturbances and failures in the SPMSM. The results showed that the proposed control performed well in the healthy mode, where SOSMC maintained smooth speed performance under various scenarios. Furthermore, the proposed FESO handled demagnetization faults effectively, achieving a significant improvement over conventional ESO approaches. In particular, the FESO reduced the mean square error by approximately 15% compared to the traditional ESO. Therefore, this FTC approach could be valuable for practical applications in various industries.

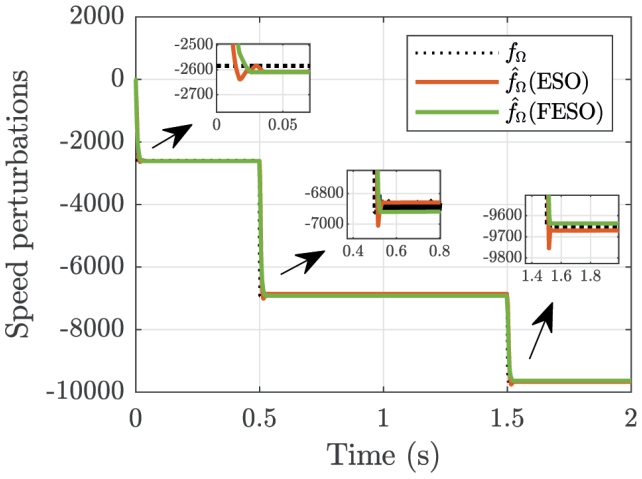

Fig. 8 The estimated value of f_Ω

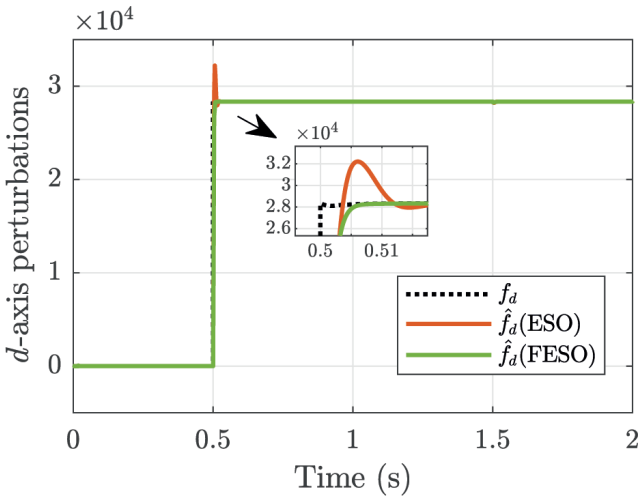

(a)

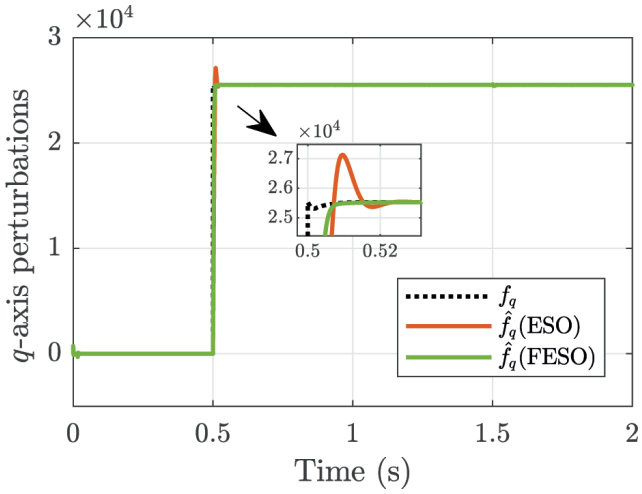

(b)

Fig. 9 The estimated values of f_d and f_q; (a) Actual value and estimation in d-axis; (b) Actual value and estimation in q-axis

Table 3 Comparison between traditional ESO and FESO

		ESO	FESO
Mean square error	$\hat{f}_\Omega$	300.8000	256.3508
	$\hat{f}_d$	747.7654	655.8482
	$\hat{f}_q$	771.2615	586.4111

References

[1] Reddy, P. B., El-Refaie, A. M., Huh, K.-K., Tangudu, J. K., Jahns, T. M. "Comparison of Interior and Surface PM Machines Equipped With Fractional-Slot Concentrated Windings for Hybrid Traction Applications", IEEE Transactions on Energy Conversion, 27(3), pp. 593-602, 2012. https://doi.org/10.1109/tec.2012.2195316

[2] Ahn, H.-J., Lee, D.-M. "A New Bumpless Rotor-Flux Position Estimation Scheme for Vector-Controlled Washing Machine", IEEE Transactions on Industrial Informatics, 12(2), pp. 466–473, 2016. https://doi.org/10.1109/tii.2016.2516974

[3] Mekki, H., Benzineb, O., Boukhetala, D., Tadjine, M., Benbouzid, M. "Sliding mode based fault detection, reconstruction and fault tolerant control scheme for motor systems", ISA Transactions, 57, pp. 340–351, 2015. https://doi.org/10.1016/j.isatra.2015.02.004

[4] Zhao, K., Zhou, R., She, J., Zhang, C., He, J., Huang, G., Li, X. "Demagnetization-Fault Reconstruction and Tolerant-Control for PMSM Using Improved SMO-Based Equivalent-Input-Disturbance Approach", IEEE/ASME Transactions on Mechatronics, 27(2), pp. 701–712, 2022. https://doi.org/10.1109/tmech.2021.3069787

[5] Han, J. "From PID to Active Disturbance Rejection Control", IEEE Transactions on Industrial Electronics, 56(3), pp. 900–906, 2009. https://doi.org/10.1109/tie.2008.2011621

[6] Liu, Z., Houari, A., Machmoum, M., Benkhoris, M.-F., Tang, T. "ESO-based FTC strategy via dual-loop compensations for 5-phase PMSG integrated tidal applications", IEICE Electronics Express, 18(20), 20210177, 2021. https://doi.org/10.1587/elex.18.20210177

[7] Qu, L., Qiao, W., Qu, L. "An Extended-State-Observer-Based Sliding-Mode Speed Control for Permanent-Magnet Synchronous Motors", IEEE Journal of Emerging and Selected Topics in Power Electronics, 9(2), pp. 1605–1613, 2021. https://doi.org/10.1109/jestpe.2020.2990442

[8] Merabet, A. "Cascade Second Order Sliding Mode Control for Permanent Magnet Synchronous Motor Drive", Electronics, 8(12), 1508, 2019. https://doi.org/10.3390/electronics8121508

[9] Zeghlache, A., Mekki, H., Djerioui, A., Benkhoris, M. F., Dahmane, N. "Fault-tolerant control of PMSM based on second-order sliding mode", In: 2022 IEEE International Conference on Electrical Sciences and Technologies in Maghreb (CISTEM), Tunis, Tunisia, 2022, pp. 1–6. ISBN 978-1-6654-5169-7 https://doi.org/10.1109/cistem55808.2022.10043923

[10] Belkhier, Y., Achour, A., Shaw, R. N., Ullah, N., Chowdhury, M. S., Techato, K. "Fuzzy Supervisory Passivity-Based High Order-Sliding Mode Control Approach for Tidal Turbine-Based Permanent Magnet Synchronous Generator Conversion System", Actuators, 10(5), 92, 2021. https://doi.org/10.3390/act10050092

[11] Sarabakha, A., Fu, C., Kayacan, E., Kumbasar, T. "Type-2 Fuzzy Logic Controllers Made Even Simpler: From Design to Deployment for UAVs", IEEE Transactions on Industrial Electronics, 65(6), pp. 5069–5077, 2018. https://doi.org/10.1109/tie.2017.2767546

[12] Moreno, J. A., Osorio, M. "A Lyapunov approach to second-order sliding mode controllers and observers", In: 2008 47th IEEE Conference on Decision and Control, Cancun, Mexico, 2008, pp. 2856–2861. ISBN 978-1-4244-3123-6 https://doi.org/10.1109/cdc.2008.4739356

[13] Yang, J., Stoll, E. "Adaptive sliding mode control for spacecraft proximity operations based on dual quaternions", Journal of Guidance, Control, and Dynamics, 42(11), pp. 2356–2368, 2019. https://doi.org/10.2514/1.g004435

[14] Kumbasar, T., Hagras, H. "Big Bang–Big Crunch optimization based interval type-2 fuzzy PID cascade controller design strategy", Information Sciences, 282, pp. 277–295, 2014. https://doi.org/10.1016/j.ins.2014.06.005

[15] MathWorks "MATLAB/Simulink, (MATLAB Online)", [computer program] Available at: https://www.mathworks.com [Accessed: 01 December 2022]

[16] Ullah, N., Farooq, Z., Sami, I., Chowdhury, M. S., Techato, K., Alkhammash, H. I. "Industrial Grade Adaptive Control Scheme for a Micro-Grid Integrated Dual Active Bridge Driven Battery Storage System", IEEE Access, 8, pp. 210435–210451, 2020. https://doi.org/10.1109/access.2020.3039947